Journal of Applied Fluid Mechanics, Vol. 12, No. 4, pp. 1287-1302, 2019.
Available online at www.jafmonline.net, ISSN 1735-3572, EISSN 1735-3645.
DOI: 10.29252/jafm.12.04.29470

Experimental and Numerical Investigation of the Efficiency and Pressure Drop of an Inertial Impactor with Variable Area

A. Namvar Ayouri[1] and M. A. Ehteram[2†]

[1] *Mechanical Engineering Department, Qom University of Technology, Qom, Iran*
[2] *Department of Mechanical and Energy, Shahid Beheshti University A.C., Tehran, Iran*

†*Corresponding Author Email: m_ehteram@sbu.ac.ir*

(Received July 27, 2018; accepted December 11, 2018)

ABSTRACT

The deposition efficiency and pressure drop of inertial impactor with variable area has been studied numerically and experimentally. The effect of volumetric flow rate, vertical barrier, oblique barrier and flexible concave plate versus deposition and impaction efficiency and pressure drop is investigated. Numerical simulation is carried out with DPM (discrete phase method) and turbulent model of SST k-ω. To validate the numerical results a special test rig is designed to study the deposition efficiency of engine oil droplets (blow-by) with a diameter of 0.1 to 6 µm. Experimental Tests are done in 8, 12, 16 and 20 L/min. To ensure the accuracy of the experimental results, all the tests are repeated at least three times for each volumetric flow rate. Gravimetric method is implemented to calculate the deposition efficiency. According to the results, the deposition efficiency is obtained between 73 and 94 percent for different mentioned impactors and different volumetric flow rate. The numerical results are confirmed by experimental results. Using the barriers increase the efficiency maximum 6 percent in different volumetric flow rate. The results show that by reducing the distance between the vertical barrier and the outlet of nozzle, the deposition and impaction efficiency are increased. Also, the Concave flexible plate with vertical barrier located at 1 mm from the outlet of nozzle is the most efficient case.

Keywords: Blow-by; Micro droplets of engine oil; inertial impactor with variable area; Pressure drop.

NOMENCLATURE

Bi	volumetric forces	u_0	velocity of air at the impactor nozzle's outlet
CD	drag coefficient	u^p	particle instantaneous velocity in axial direction
d_p	particle diameter	u'	fluctuating velocity
d_{ij}	deformation tensor	$\overline{u}$	mean velocity
F_i	Saffman force	V	relative velocity
F^L	lift force	xi	data
g_i	acceleration due to gravity	$\overline{x}$	arithmetic mean
k	turbulent kinetic energy	β^*	closure coefficient in the turbulence-kinetic-energy equation
L	length scale	κ	Favare_averaged specific turbulence kinetic energy
L_t	characteristic length	$\dot{\gamma}$	shear rate
N	number of data	ζ	normally distributed random number
P	particle	η_d	deposition efficiency
P	mean static pressure	η_i	impaction efficiency
r	the particle radius		
Re_D	Reynolds number		
St	stock number		
T_L	Lagrangian integral time scale		
T	time		
u	instantaneous velocity		
u_p	velocity of the particle		

μt	turbulent viscosity
μ	dynamic viscosity
ν	kinetic viscosity
ρ	gas density
ρ	Mean mass density
σ	standard deviation
τ	particle relaxation time
τ_e	random variation
τ_{ij}	Favre-averaged specific Reynolds-stress tensor
ω	specific dissipation rate
σ , β , σ_d	closure coefficient in the specific dissipation-rate equation

1. INTRODUCTION

The gas flow containing droplets is one of the most important branches of multiphase flows. In this type of flows, the study of droplets motion, growth and deposition on solid wall is extremely significant. The separation of droplets from two-phase flows is requested in many industrial applications. The separation of water and oil droplets from air in the compressed air, separation of mixed water droplets in wet scrubber, separation of water droplet on cooling tower and separation of oil droplets in crankcase ventilation system in spark ignition engines are some examples of this field. With regarding to the limitation of engine exhaust emissions, researchers are interested in obtaining the maximum decrease of engine pollutant. One of these pollutants is the oil consumption inside the motors which could give rise to catalyst poisoning, defective combustion and provide deposits on different parts of engine. During the combustion process, some gas flow escapes beside piston gaps to the crankcase which is named Blow-by. In order to decrease this emission, the leakage gas is returned into the intake manifold which is cleaned enough to use in the combustion process. the unsuitable crankcase ventilation system could lead to an increase of oil burned by the engine (De La Mora, Rao *et al*. 1990, Kim *et al*. 2014). As ultrafine oil droplets exist in the crankcase vapors, it is necessary to separate the oil droplets from the vapors before they return to the combustion chamber. Oil separating is implemented with different methods like inertial impactor and cyclone. Pagnozzi, Pereira *et al*. (2007) applied a methodology to validate a standard air/oil separation system (AOS) for a 7.2liter diesel engine. Feng *et al*. (2008) investigated on the separation efficiency of the horizontal oil-gas separator, which is widely used in the oil-injected compressor units. They also applied a (Malvern) technique to measure the oil concentration and separation efficiency. They found that the separation efficiency is raised by increasing the oil injection flow rate. Movafaghian *et al*. (2000) studied on the hydrodynamic flow behavior of a Gas–Liquid Cylindrical Cyclone for a different inlet geometry experimentally and theoretically. They refined an existing GLCC mechanistic model. They also compared their modified model predictions with experimental data which had very good agreement (Arpandi *et al*., 1996, Movafaghian *et al*. 2000). A low-pressure impactor with eight-stage is considered with 50% efficiency cut-off size 4.0, 2.0, 1.0, 0.05, 0.26, 0.11, 0.075, and 0.05-μm aerodynamic diameter (Hering *et al*. 1978). Fernandez *et al*. (de la Mora *et al*. 1990) studied inertial impaction process of fine particles in transonic gas flow regimes using a thin-plate orifice nozzle. They pointed out that there is no fluid dynamic ban for the inertial collection of the ultrafine particles (Ashkenas, 1966, de la Mora, Hering *et al*. 1990). Ishii *et al*. (1989) investigated the inviscid supersonic flows around truncated cylinders and Forney (1991) performed a similar study for a viscous supersonic flow using the axisymmetric compressible Navier–Stokes equations. They also considered the thermophoresis effect in their analysis of particle deposition process (Forney 1991, Oh and Kim 1994). Rajmistry *et al*. (Rajmistry *et al*. 2017) studied the gas-solid flow in a cyclone attached to the CFB system numerically. This study included critical parameter such as coefficient of restitution which is responsible for swirling effect and increase in efficiency. The results showed the efficiency of the cyclone was dependent on particle size and coefficient of restitution. Hung-Ying Chen *et al* (Chen and Huang 2016) presented an innovative active virtual impactor (AVI) to separate particles. The operation parameters of different flow rates regarding sample flow velocity, side flow velocity, and sheath flow velocity were considered numerically and experimentally. The results showed that particles were increasingly separated when the side flow velocity increased. Ehteram *et al*. (2012) investigated the effect of cyclone inlet configuration on oil droplets impaction efficiency in different geometry like circle, triangle, rectangle with 14mm hydraulic diameter. The results showed that rectangle and triangle geometries have a better efficiency toward circle ones in the same hydraulic diameter. Although many experiments have been done to develop the oil particles inertial impactors, Satoh *et al*. (2000) investigated the efficiency and optimization of the inertial impactors with the method of computational fluid dynamic(CFD). Ehteram *et al*. (2013) introduced a new method for producing of micron droplets with impacting an air jet to the surface of engine oil. Gas permeation into the oil surface leads to formation of oil strings and with impacting the air jet to these strings, the ultrafine droplets form with the diameter less than 5 micrometers. Shojaeefard *et al*. (2015) studied on the deposition of ultrafine oil particles on circular inertial impactor. The numerical and experimental investigation of the effect of ultrafine oil particles with 0.1–6 μm diameter which has deposited on the cold flat plate is done by Shojaeefard *et al*. (2016). They also considered the effect of flow velocity and droplet size on the deposition efficiency.

In the current work, a new inertial impactor is designed and constructed to separate the oil particles from the two phase flow which named inertial impactor with variable area. the impaction and deposition efficiency and pressure drop of the inertial impactor with variable area simple is considered numerically. To validate the numerical results, a special test rig is designed to study the deposition efficiency of engine oil droplets with diameters of 0.1 to 10 μm of gas leakage (blow-by) experimentally. Also, to improve deposition efficiency of inertial impactor, three optimized patterns with vertical and oblique barrier and concave flexible plate are designed and their performance are investigated numerically and experimentally.

2. MATERIAL AND METHODS

2.1 Designed Inertial Impactor with Variable area

In case where the volumetric flow rate is changing, the deposition efficiency of inertial impactor is not effective because of constant distance between the outlet of the nozzle and the plate. In this study, a new method is used to increase the deposition efficiency of oil particles. For this purpose, an inertial is designed and constructed and named inertial impactor with variable area. In the inertial impactor with variable area, distance between the outlet of nozzle and the plate varies by passing different volumetric flow rates through the impactor. The distance between the outlet of nozzle and the plate is an important issue in the impaction of droplet to the surface (Alatawia and Matidaa, 2012). At the beginning there is no flow, so the distance between flexible plate and outlet of nozzle is equal to zero. With starting the flow, according to the flow rate the amount of force on the flexible plate was increased and subsequently the distance between the flexible plate and the nozzle was increased. When flow passes through the plate it is accelerated and reached their maximum velocity. The most effective factor to deposit the droplets is their velocity. The velocity gives rise to deposition, rebounding or splashing (droplets become smaller) of droplets. Hence, the amount of wettability of the surface is defined and a liquid film is formed on the plate (Gavaises *et al.* 1996). Inertial impactor with variable area separates the oil particles in two steps. The flexible plate plays the principal role of separation and the wall of exit channel is the second separator (Fig. 1a). To improve the deposition efficiency of inertial impactor, two optimized impactors with vertical and oblique barrier are designed and considered experimentally and numerically. Angle of oblique barrier is 70 degrees (Fig. 1b, c).These barriers play the third role of separation. Flexible plate has two duties. The first one is as a separator and the second one is as a check valve that prevents the flow return. Finally an optimized design, inertial impactor with variable area with vertical barrier and concave flexible plate is represented and considered numerically (Fig. 1d).

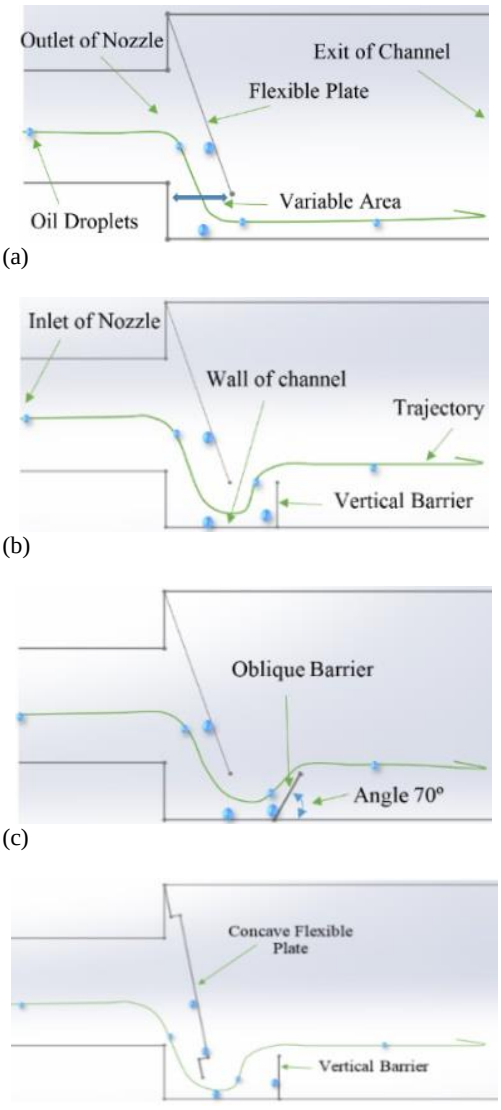

Fig. 1. Schematic of Inertial impactor with variable area: (a) simple (b) with vertical barrier and (c) with oblique barrier (d) vertical barrier and concave flexible plate.

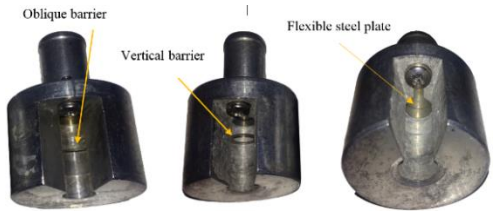

Fig. 2. Sample made (a) inertial impactor with variable area simple (b) with vertical barrier (c) with oblique barrier.

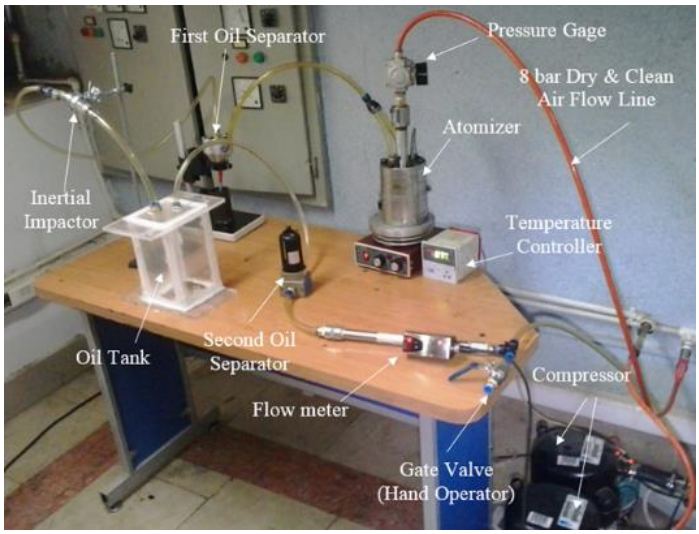

Fig. 3. Experimental test rig.

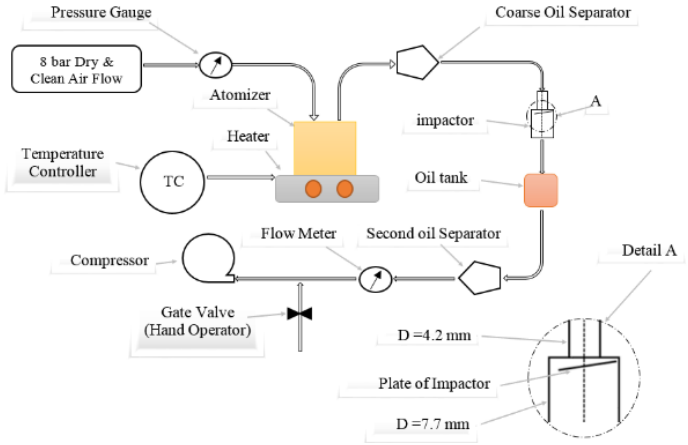

Fig. 4. Schematic of the experimental apparatus.

2.2 Experimental Apparatus

Due to the fluctuations in engine speed and the engine power, the high expense of engine test, less reliability and less repeatability in comparison with laboratory method, an experimental test rig was designed to consider the deposition efficiency of inertial impactor with variable area, basically. The experimental test rig is included an engine oil droplet generator (atomizer) and an inertial impactor with variable area that is shown in Fig. 3 and Fig.4.

To generate a distribution of oil droplets in the same size as the oil droplets in blow-by gases of IC engines, an atomizer was designed (Ehteram, *et al*. 2013). Fig. 5 shows the number and mass fractions of droplets. The distribution is same as oil droplets in blow-by gases in engine. The diameter of droplets is smaller than 6 µm and average diameter (Sutter diameter) is about 1.2 µm.

Since the concentration of oil particles in two phase flow was less than 5 percent (Crowe *et al*. 2011), the flow was noticed to be diluted. Therefore, reduction of nozzle diameter does not have an effect on the droplet size distribution and collisions between the droplets. So distribution of the droplets was considered according to Fig.5.

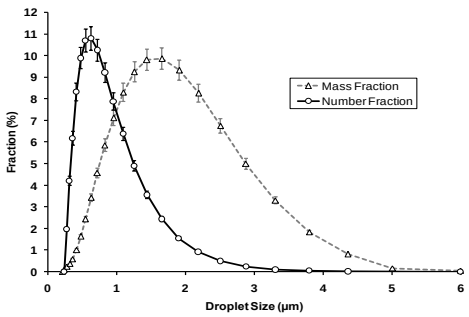

Fig. 5. Oil droplet size distribution(Ehteram *et al*. 2013).

2.2 Test Procedure

At the beginning of each test, enough oil must be poured into the atomizer to maintain the level of oil. Also, all equipment must be cleaned and dried. Besides, all the equipment and interface hoses must be weighed. After all equipment, systems and connections were checked, the test was started. At first, the tests were performed in

the period of one hour, but because the accuracy of the used scale was ± 0.1mg, the collected weight of oil particles was not tangible. So, the time of each test was increased to two hours. Gravimetric method was employed to estimate the deposition efficiency. After preparing and weighing all equipment, the test rig was assembled as shown in Fig. 3 and Fig. 4. Then the electrical heater was turned on to heat the oil inside the atomizer to 90 ºC, as warm as the oil inside the engine of a car. Next, the valve of dried air 8 Bar was opened to circulate the flow and start the test. To eliminate the oscillation of compressor suction, the length of connecting hose to the compressor was considered long enough. The Volumetric flow rates used in this experimental test are 8, 12, 16 and 20 L/min (same as flow rate of blow-by in IC engine) and this was adjusted by a gate valve (hand operator). After 2 hours the compressor was turned off and then all equipment consisting of coarse oil separator, impactor, oil tank, second oil separator, connecting hoses and atomizer were weighed again to obtain the deposition efficiency. One of the important points in the experimental tests is repeatability of the test results. To ensure the accuracy of the results of the designed test rig, all the experiments were repeated at least three times for each volumetric flow rate. According to repeated tests, minimum and maximum experimental uncertainty were obtained 0.36 and 11.07 percent, respectively.

$$\bar{X} = \frac{1}{n}\sum_{i=1}^{n} X_i \tag{1}$$

$$\sigma = \left[\frac{1}{n}\sum_{i=1}^{n}(x_i - \bar{x})^2\right]^{\frac{1}{2}} \times 100 \tag{2}$$

In the above equation, $\bar{X}$ is the arithmetic mean, n the number of repeated tests or the number of data, xi data and σ is the standard deviation (experimental uncertainty). Engine lubricant oil 10W40 was used in the tests. Properties of the oil are shown in Table 1.

Table 1: Engine oil (10W40) analysis (Shojaeefard, Khaneshan *et al.* 2016)

Property	Unit	Quantity
Viscosity@40°C	cSt	104
Total Base Number	mg KOH/g	9.79
Metal Content		
Iron(Fe)	ppm	0.80
Aluminum(Al)	ppm	1.10
Copper(Cu)	ppm	0.10
Magnesium(Mg)	ppm	18.00
Zinc(Zn)	ppm	1338.00
Phosphor(P)	ppm	998.00
Barium(Ba)	ppm	0.20

To calculate pressure drop of the impactor, two digital pressure gauges with accuracy of ±20 Pascal were placed before and after the impactor. Fig. 6 shows the experimental test rig for pressure drop calculation.

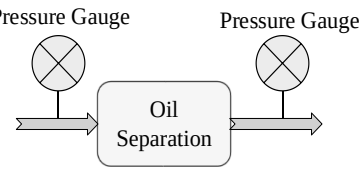

Fig. 6. Experimental test rig for pressure drop.

2.3 Numerical Description

In this paper, a model is developed to study the transport and deposition of droplets in the impactor. For this purpose, a numerical in-house code is used.

2.3.1 Governing Equations and Turbulence Modeling

$$\frac{\partial \rho}{\partial t} + \frac{\partial (\rho \overline{u_i})}{\partial x_i} = 0 \tag{3}$$

$$\rho\left[\frac{\partial \overline{u_i}}{\partial t} + \overline{u_j}\frac{\partial \overline{u_i}}{\partial x_j}\right] = \overline{B_i} - \frac{\partial \overline{P}}{\partial x_i} + \frac{\partial}{\partial x_j}\left[\mu\frac{\partial \overline{u_i}}{\partial t} - \overline{\rho u_i' u_j'}\right] \tag{4}$$

The equations are verified for all experiments. In the above equation, ρ is the fluid density, Bi is volumetric forces and μ is the dynamic viscosity, $\bar{u}$ and u' represent mean and fluctuating velocities respectively, and the instantaneous velocity is $u_i = \bar{u}_i + u_i'$.

The term of $\rho\overline{u_i' u_j'}$ is called Reynolds stress tensor which is calculated by the Eq. (5).

$$-\rho\overline{u_i' u_i'} = \mu_t\left(\frac{\partial U_i}{\partial x_j} + \frac{\partial U_j}{\partial x_i}\right) - \frac{2}{3}\rho k\,\delta_{ij} \tag{5}$$

Where the turbulent kinetic energy, $k = \frac{1}{2}\left(\overline{u'^2} + \overline{v'^2} + \overline{\omega'^2}\right)$; μ_t is the turbulent viscosity and typically calculated as a function of one or two transport variable.

The SST two equation turbulence model was introduced in 1994 by F.R. Menter to deal with the strong freestream sensitivity of the k-omega turbulence model and improve the predictions of adverse pressure gradients (Menter 1994).

The turbulent viscosity μ_t, as needed in the RANS equations, is given by: $\mu_t = Vt^* \rho = f(k,\omega)$ while the evolution of k and ω is modelled as:

For recommendations for the values of the different parameters, see (Menter 1994).

$$\frac{\partial(\rho\kappa)}{\partial t}+\frac{\partial(\rho u_j\kappa)}{\partial x_j}=P-\beta^*\rho\omega\kappa+\frac{\partial}{\partial x_j}\left[(\mu+\sigma_k\mu_t)\frac{\partial\kappa}{\partial x_j}\right] \quad (6)$$

$$\frac{\partial(\rho\omega)}{\partial t}+\frac{\partial(\rho u_j\omega)}{\partial x_j}=\frac{\gamma}{\nu_t}P-\beta\rho\omega^2+\frac{\partial}{\partial x_j}\left[(\mu+\sigma_\omega\mu_t)\frac{\partial\omega}{\partial x_j}\right]+2(1-F_1)\frac{\rho\sigma_{\omega2}}{\omega}\frac{\partial\kappa}{\partial x_j}\frac{\partial\omega}{\partial x_j} \quad (7)$$

Where κ is Favare_averaged specific turbulence kinetic energy, P mean static pressure, β^* is closure coefficient in the turbulence-kinetic-energy equation, ω is specific dissipation rate, β is closure coefficient in the specific dissipation-rate equation, τ_{ij} is Favre-averaged specific Reynolds-stress tensor.

2.3.2 Description of Computational Domain and Methodology

Designing solution domain's control volume is the first step of simulation the principle phase flow field. Control Volume's boundary condition is composed of the input, output parts, flexible plate and walls (with no-slip condition) (Fig.7).

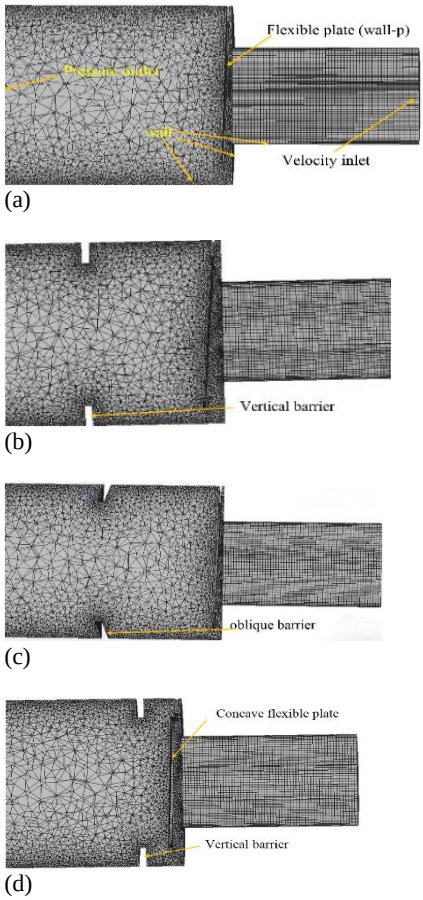

Fig. 7. Inertial impactor with variable area meshing in 8 L/min flow rate (a) simple (b) with vertical barrier (c) with oblique barrier (d) with vertical barrier and concave flexible plate.

Due to the importance of boundary layer in deposition of droplets, the mesh was refined (made smaller) in some areas such as the impaction nozzle's outlet, distance between the flexible plate and the impaction nozzle, near the flexible plate and near the walls. The boundary conditions include the velocity inlet at the entrance of the impactor nozzle, pressure outlet at the impactor exit and no-slip at the walls. The velocity of droplets and air at the inlet of the nozzle were assumed to be the same as each other and are constant. The pressure outlet is the same as the vacuum pressure of the compressor in the experimental test. The distribution of injected droplets from the nozzle's inlet was the same as Fig.5. The flow was considered to be incompressible; since the flow was diluted, the density of the flow was supposed to be constant. The Pressure Implicit With Splitting of Operators (PISO) algorithm was applied for coupling of momentum and continuity equations (Issa 1986). Solving the problems of an impinging jet was well executed by this method (Bazdidi-Tehrani *et al.* 2011). Second-order upstream discretization was used for discretization of equations. Discrete phase modeling (DPM) and Lagrangian approach were implemented for particle tracking. Since the Lagrangian approach was used, each single particle was traceable. As mentioned before, the flow was considered to be diluted so interaction between particles was not considered. The equation of motion for a spherical particle in a gas is given by Eq.8:

$$\frac{du_i^p}{dt}=\frac{1}{\tau}\frac{C_D\,\mathrm{Re}_D}{24}(u_i-u_i^p)+\frac{g_i(\rho_p-\rho)}{\rho_p}+F_i^L \quad (8)$$

Where, $\frac{g_i(\rho_p-\rho)}{\rho_p}$ is known as the effect of the gravity on the droplets, $\tau=\frac{\rho_p d_p^2}{18\mu}$ is known as particle relaxation time.

The Saffman force can be expressed

$$F_i=K\mu\mathcal{N}r^2(\dot{\gamma}/\nu)^{1/2} \quad (9)$$

Where constant K=81.2, r is the particle radius, $V=u_i-u_{ip}$ is the relative velocity, $\dot{\gamma}$ is the shear rate and ν is the kinetic viscosity (Saffman 1965).

In the Eq.8, the flow velocity u_i can be described as

$$u_i=\bar{u}_i+u_i'$$

The discrete random walk (DRW) method, implemented to show the interaction of eddies with the droplets, was included through the work of Hutchinson, Hewitt *et al.* (1971) and completed by Kallio and Reeks (1989).in this study, a discrete random walk (DRW) model based on stochastic method was used to determine the fluctuating gas velocity. The values of fluctuating velocities that

prevail during the lifetime of a turbulent eddy τe, are sampled by assuming that they obey a Gaussian probability distribution using correlation as:

$$u_i' = \zeta\sqrt{\overline{u_i' u_j'}} \tag{10}$$

Where ζ is a normally distributed random number and the term $\sqrt{\overline{u_i' u_j'}}$ is local root mean square (RMS) of velocity fluctuations. In the present study, the characteristic life time τ_e of an eddy was calculated as random variation about the Lagrangian integral time scale T_L , using following expression

$$\tau_e = -T_L \ln(r) \tag{11}$$

Where r is a random number between 0 and 1 and $T_L = 0.3K/\varepsilon$ (Shukla *et al*. 2011).

The drag coefficient , C_D = 0.44 can be discerned for high Reynolds number of droplets (Petkov *et al*. 1995). Because the place of droplets was dependent on the time, this problem is unsteady, therefore, stability of the system must be checked according to the time step chosen. Time step was noticed according to Eq. 12.

$$\Delta t = \frac{L}{u_p + u_0} \tag{12}$$

Where the length scale (the distance that droplets travel in each time step) was shown by L, u_0 is the velocity of air at the impactor nozzle's outlet (Fig. 1a) and u_p is recognized as droplet velocity. The location of the particles will be updated at the end of each step because the solving is decoupled. Because the two-phase flow was assumed to be diluted the droplet had a minimal effect on the flow, so this effect can be deleted and OWC (One Way Coupling) was applied. Droplets were injected in each numerical run according to the distribution shown in Fig. 5.

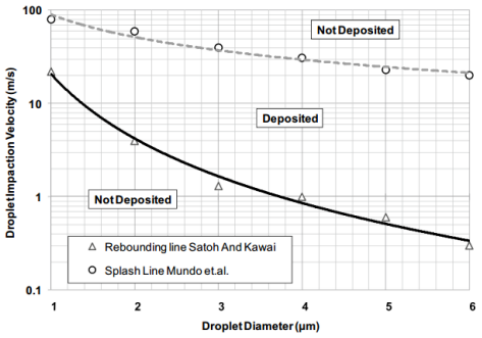

Fig. 8. Deposited and not deposited area according to droplet diameter (Shojaeefard *et al.* 2016).

Fig. 8 shows deposited and not deposited area according to droplets size and perpendicular droplets impaction velocity to the collision surface (Shojaeefard *et al*. 2016). In the written code it was assumed the droplets located inside the deposition area were deposited and outside of this area were rebounded from the surface and were not deposited. The flowchart of the numerical in-house code was represented in Fig. 9 and convergence was checked by computing the residual error of 10^{-4}, generally. Turbulence intensity at the inlet and outlet flow was considered to be 5.5 %.

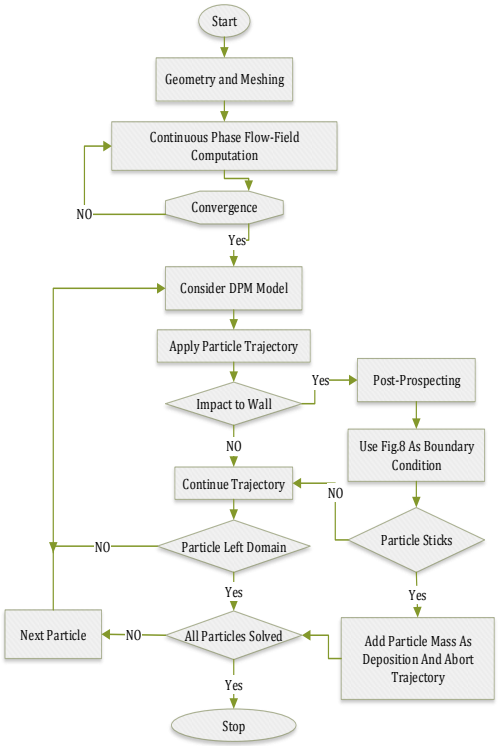

Fig. 9. Code diagram.

The impaction and deposition efficiency are calculated by Eq. 13 and Eq. 14 respectively.

$$\eta_i = \frac{Mass\ of\ oil\ droplets\ impacted\ on\ inertial\ impactor}{Mass\ of\ oil\ droplets\ injected\ from\ interance\ nozzle} \tag{13}$$

$$\eta_d = \frac{Mass\ of\ oil\ droplets\ deposited\ on\ inertial\ impactor}{Mass\ of\ oil\ droplets\ injected\ from\ interance\ nozzle} \tag{14}$$

Where η_i is impaction efficiency and η_d is deposition efficiency. The mass of the injected and deposited oil droplets was obtained by weighing the atomizer, impactor and all equipment between the atomizer and impactor before and after each test as mentioned before. Droplet deposition means the droplets trapped after impaction onto the surface. According to the droplets size (Fig. 5) and impaction velocity, they can form a thin liquid layer of oil or can remain as a droplet. Impaction efficiency can just be obtained in numerical simulation. Deposition and

Table 2: 3-D Numerical simulations and experimental tests

	Inertial impactors	Volumetric Flow Rate(L/MIN)				
		3	8	12	16	20
3-D Numerical simulation	Inertial Impactor with Variable Area, Simple	*	*	*	*	*
	Inertial Impactor with Variable Area with vertical barrier. The barrier was located at 5 mm distance from the outlet of nozzle		*			*
	Inertial Impactor with Variable Area with vertical barrier. the barrier was located at 3 mm distance from the outlet of nozzle		*			
	Inertial Impactor with Variable Area with vertical barrier. The barrier was located at 1 mm distance from the outlet of nozzle		*			
	Inertial Impactor with Variable Area with oblique barrier. The barrier was located at 5 mm distance from the outlet of nozzle		*			*
	Inertial Impactor with Variable Area with vertical barrier and concave flexible plate. The barrier was located at 1 mm distance from outlet of nozzle		*			
Experimental Tests	Inertial Impactor with Variable Area, Simple		*	*	*	*
	Inertial Impactor with Variable Area with vertical barrier. The barrier was located at 5 mm distance from the outlet of nozzle		*			*
	Inertial Impactor with Variable Area with oblique barrier. The barrier was located at 5 mm distance from the outlet of nozzle		*			*

Impaction efficiencies are related to droplet velocity and droplet size. a proper way of showing impaction and deposition on the plate is obtained by (Shojaeefard *et al*. 2016) versus Stokes number. Stokes number is the ratio of particle/droplet inertial forces versus the viscous forces. therefore Stokes number can show the particle/droplet's tendency to follow their original path (Kim *et al*. 2014). The Stokes number equation is given by Eq.15.

$$St = \frac{\tau U_0}{L_t} = \rho_p d_p{}^2 U_0 \Big/ 18\mu L_t \qquad (15)$$

In the above equation, τ is the particle relaxation time, u_o is air velocity at impactor nozzle's outlet and d_p and ρ_p are the particle/droplet's diameter and density respectively, and μ is the dynamic viscosity of air and Lt is the characteristic length.

3. Results And Discussion

3.1 List of Numerical Simulation and Experimental Tests

The 3-D numerical simulation and experimental test are presented in Table 2.

3.2 Evaluation of mesh independence

According to the average velocities at the outlet of nozzle (Fig. 1a), the mesh-independent results were performed between 374119 nodes and 556114 nodes. The results show that average velocity for meshes more than 435023 nodes remains almost constant; therefore, for all of the numerical simulations the number of nodes was applied to 435023 nodes. Fig. 10 shows the Mesh independency results.

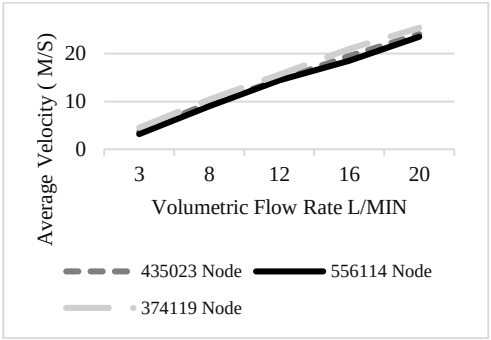

Fig. 10. Mesh Indecency for inertial impactor with variable area simple for constant angle of flexible plate in different flow rate.

3.3 Continuous phase simulation

In order to identify the continuous phase, the air jet characteristic in the impactor is investigated numerically. Fig. 11 shows the numerical simulation of air jet velocity in 8 L/min flow rate for inertial impactor with variable area simple.

3.4 Particles Tracking

Due to the experimental setup limitation and inaccessibility of an appropriate apparatus for high speed photography of micro particles, the particle tracking is only done by numerical simulation. After simulation of continuous phase, Eq.8 was solved to track the particles. Mono-sized particles with diameter of 1-6 µm were injected from the inlet of nozzle uniformly. Mass fraction of every particle size is achieved from Fig.5. The particle tracking on the inertial impactor with variable area simple at 8 L/min volumetric flow rate is shown in Fig. 12. The results showed that the ultrafine particles followed the air flow line, while the larger particles preferred to continue their direction due to higher inertia. The larger particles would not change their direction with changing in carrier flow direction near the flexible plate. As shown in Fig. 12, most of the particles with diameter of 0.3 and 0.7 µm have followed the carrier flow direction. Some of the droplets with diameter of 0.3 and 0.7 µm have separated with flexible plate and others separated with wall of exit channel. About 90% of particles with 1 µm diameter have been separated by flexible plate and wall of exit channel. The particles with 2 µm diameter and larger than 2 µm have been completely separated by flexible plate (100 %). Fig. 13 shows the particles tracking of inertial impactor with variable area, with vertical barrier in 8 L/min volumetric flow rate. The vertical barrier was located at 5 mm distance from the outlet of nozzle. The particles with diameter of more than 2 µm have completely separated from the flow. Therefore, it has been ignored in order to show their contours. Fig. 14 shows the particles tracking of inertial impactor with oblique barrier in 8 L/min flow rate. Oblique barrier is located at 5mm distance from the outlet of nozzle. Fig. 15 shows the particles tracking of inertial impactor with variable area, with vertical barrier and concave flexible plate in 8 L/min flow rate. The vertical barrier was located at 1 mm distance from the outlet of nozzle.

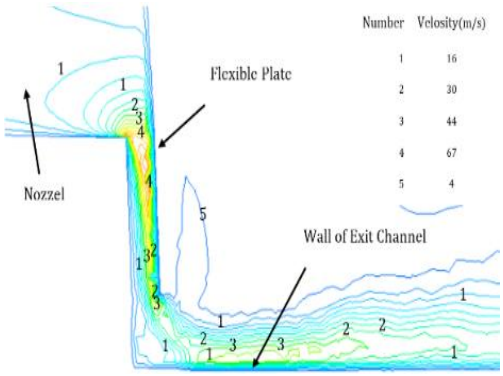

Fig. 11. Numerical simulation of air jet velocity in 8 L/min volumetric flow rate for inertial impactor with variable area simple.

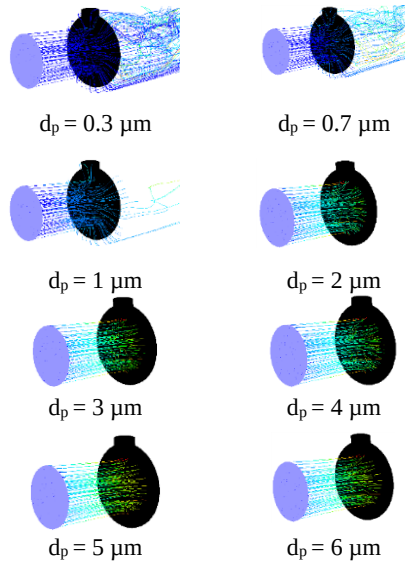

Fig. 12. Particle tracking of inertial impactor with variable area simple in 8 L/min volumetric flow rate.

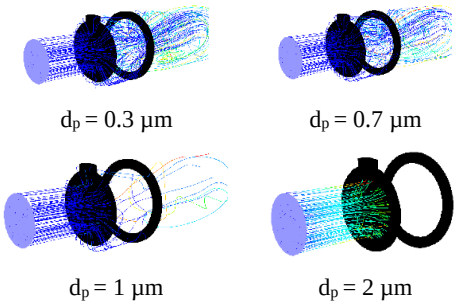

Fig. 13. Particle tracking of inertial impactor with variable area with vertical barrier in 8 L/min volumetric flow rate. The barrier was located ta 5mm distance from the outlet of nozzle.

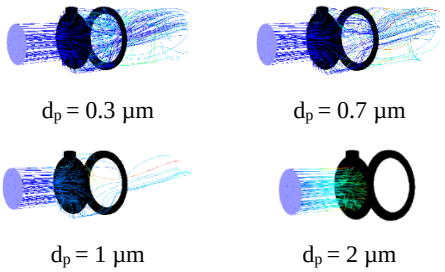

Fig. 14. Particle tracking of inertial impactor with variable area, with oblique barrier in 8 L/min flow rate. The barrier was located at 5mm distance from the outlet of nozzle.

3.5 Impaction and Deposition Efficiencies Numerically

Fig. 16 (a) and (b) show the Impaction and deposition efficiency respectively for inertial impactor with variable area simple, with vertical barrier and oblique barrier numerically. The vertical and oblique barrier was located at 5 mm from the outlet of nozzle. According to Fig. 16 (a), the impaction efficiency of inertial impactor with

variable area simple at 3, 8, 12, 16 and 20 L/min volumetric flow rate is reported 75, 85, 87, 88 and 92 percent respectively. The result shows that with increasing the flow rate, the impaction efficiency is increased. The impaction efficiency for 8 and 20 L/min volumetric flow rate is reported 92 and 95 percent for impactor with vertical barrier (located at 5 mm from the outlet of nozzle) and 86 and 93 percent for impactor with oblique barrier (located at 5 mm from the outlet of nozzle) respectively. According to Fig .16 (b), the deposition efficiency of inertial impactor with variable area simple for 3, 8, 12, 16 and 20 L/min volumetric flow rate is reported 73, 84, 87, 87 and 91 percent respectively. Also, the deposition efficiency for 8 and 20 L/min flow rate is reported 91 and 94 percent for inertial impactor with variable area with vertical barrier (located at 5 mm from the outlet of nozzle) and 85 and 92 percent for inertial impactor with variable area with oblique barrier (located at 5 mm from outlet of nozzle) respectively. There are some particles that impacted to the wall and rebounded due to their high velocity. So, the deposition efficiency is less than the impaction ones. According to tracking particle (Fig. 12), droplets with diameters more than 1µm were totally separated. So, vertical and oblique barriers were used to separate the droplets with diameter less than 1µm. According to Fig. 5, droplets with diameter less than 1µm have a little portion of mass fraction in comparison with droplets with diameter more than 1µm. Therefore, using barriers has little effect on the deposition and impaction efficiency.

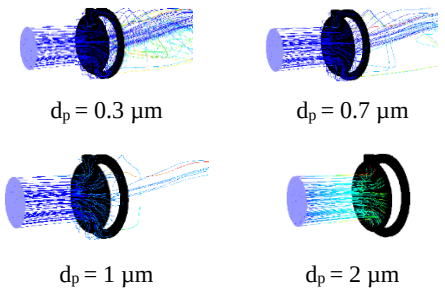

Fig. 15. Particle tracking of inertial impactor with variable area, with vertical barrier and concave flexible plate in 8 L/min flow rate. The barrier was located at 1mm distance from the outlet of nozzle.

3.6 The Comparison of Numerical and Experimental Results of Deposition Efficiency

Fig. 17 shows the comparison of numerical simulation and experimental result for inertial impactor with variable area simple. The numerical simulation of oil droplets deposition efficiency for 8, 12, 16 and 20 L/min volumetric flow rate is reported 84, 87, 87 and 91 percent and for experimental results is reported 78, 85, 85 and 86 percent respectively. The experimental results conform the numerical simulations.

Fig. 18 shows the comparison of numerical simulation and experimental result for inertial impactor with variable area with vertical barrier at 5mm distance from outlet of nozzle. The numerical simulation of oil droplets deposition efficiency for 8 and 20 L/min volumetric flow rate is reported 91 and 94 percent and for experimental results is reported 84 and 86 percent respectively.

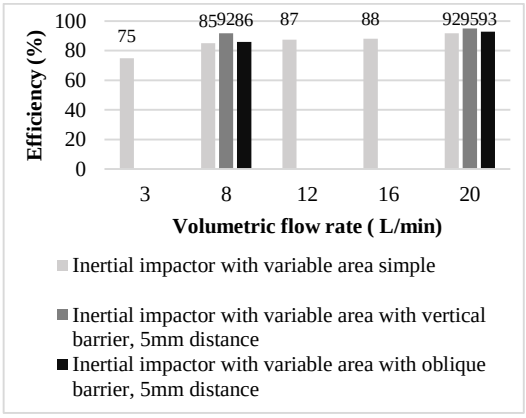

(a)

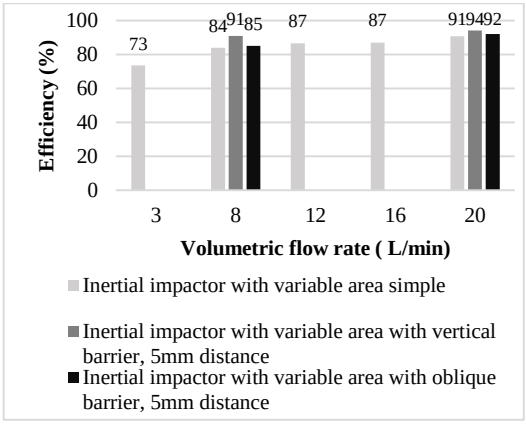

(b)

Fig. 16. (a)The impaction efficiency (b) deposition efficiency for different volumetric flow rate numerically.

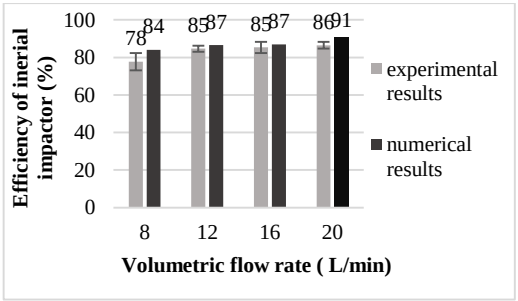

Fig. 17. Comparison of numerical simulation and experimental result of deposition efficiency for inertial impactor with variable area simple.

Fig. 19 shows the comparison of numerical simulation and experimental result for inertial

impactor with variable area with oblique barrier at 5mm distance from the outlet of nozzle. The numerical simulation of oil droplets deposition efficiency for 8 and 20 L/min volumetric flow rate are reported 85 and 92 percent and for experimental results are reported 84 and 86 percent respectively. All results show that the numerical simulations have good adaptation with the experimental results.

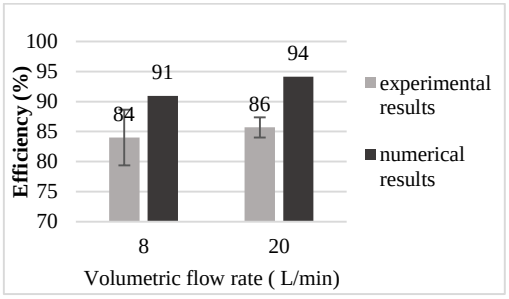

Fig. 18. Comparison of numerical simulation and experimental result of deposition efficiency for inertial impactor with variable area with vertical barrier at 5mm distance from the outlet of nozzle.

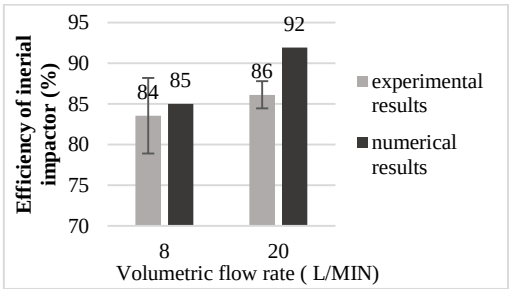

Fig. 19. Comparison of numerical simulation and experimental result of deposition efficiency for inertial impactor with variable area with oblique barrier at 5mm distance from outlet of nozzle.

3.7 The Numerical Deposition Efficiency for Different Size of Droplets

Fig. 20 shows the deposition efficiency for different size of droplets in different segments of inertial impactor with variable area simple in 8 L/min volumetric flow rate numerically. The droplets with diameter larger than 1µm were separated with flexible plate totally and their deposition efficiency are reported 100 percent. So the deposition efficiency of wall of exit channel equal to zero. The main problem of inertial impactor is the separation of particles with diameter less than 1 µm. The deposition efficiency of particles with diameter 0.3, 0.7 and 1 µm was reported 5, 10 and 44 percent for flexible plate and 7, 33 and 45 percent for wall of exit channel respectively. The total deposition efficiency of particles with diameter of 0.3, 0.7 and 1 µm was reported 11, 43 and 89 percent respectively. As shown in Fig. 20, the wall of exit channel plays the prominent role to separate the particles with diameter less than 1µm. The results show that the deposition efficiency for particles with diameter less than 0.7 µm is less than 50 percent.

3.8 The Effect of Distance Between Barriers and Outlet of Nozzle on Impaction and Deposition Efficiency Numerically

Fig. 21 shows the schematic of inertial impactor with variable area, with vertical barrier. Regarding to Fig. 21, three different distances between vertical barrier and outlet of nozzle, 1, 3 and 5 mm, have been investigated. Fig. 22 shows the effect of distance between barrier and outlet of nozzle on impaction and deposition efficiency in 8 L/min volumetric flow rate numerically. According to the Fig. 22, the impaction efficiency for 1, 3 and 5 mm distance of vertical barrier in 8 L/min flow rate is reported 92, 92 and 91 percent and the deposition efficiency is reported 92, 91 and 90 percent respectively. The result shows that with decreasing the distance between vertical barriers and outlet of nozzle, the efficiencies will be increased. The impaction and deposition efficiency for inertial impactor with variable area with oblique barrier (located at 5 mm from the outlet of nozzle) were obtained 86 and 85 percent respectively. Fig. 22 also shows the results for another optimized design in which flexible plate is concave and the distance between vertical barrier and the outlet of the nozzle is 1 mm. The results show that deposition and impaction efficiency are 93 and 93 percent in 8 L/min flow rate respectively.

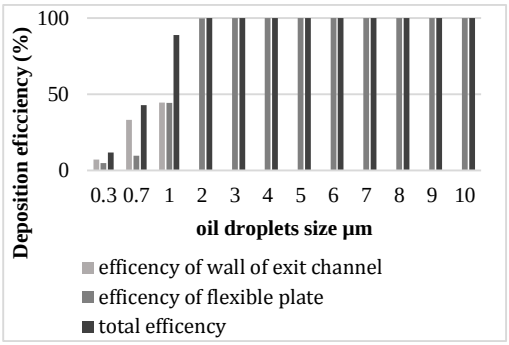

Fig. 20. Deposition efficiency for different size of droplets in different part of inertial impactor with variable area simple in 8 L/min flow rate numerically.

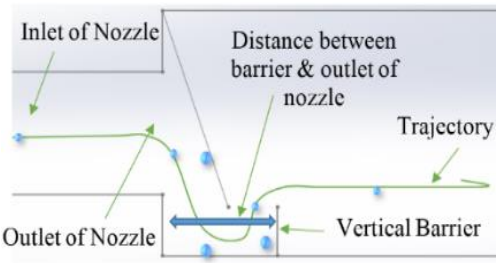

Fig. 21. Schematic of inertial impactor with variable area with vertical barrier, and the distance between barrier & outlet of nozzle is shown.

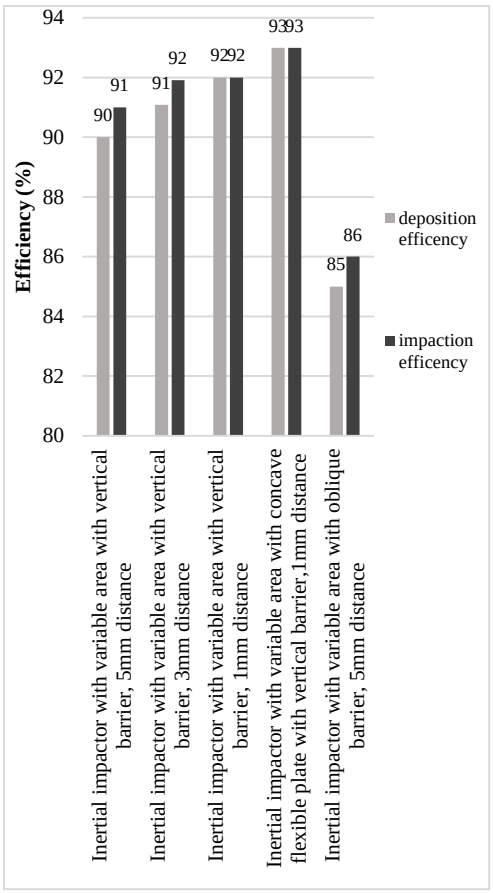

Fig. 22. Effect of distance between barriers and outlet of nozzle on impaction and deposition efficiency in 8 L/min numerically.

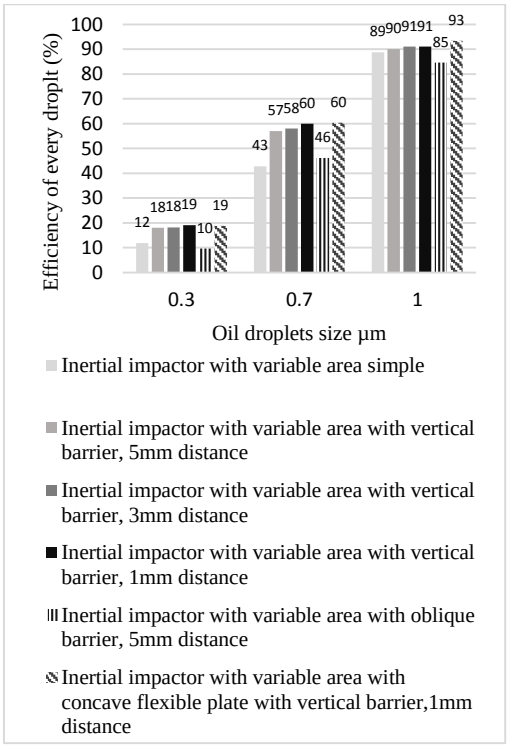

Fig. 23. Droplets deposition efficiency with diameter of 0.3, 0.7 and 1 µm in 8 L/min volumetric flow rate numerically.

Fig. 23 shows the droplets deposition efficiency with diameter of 0.3, 0.7 and 1 µm in 8 L/min flow rate numerically. As the deposition efficiency of particles with diameter larger than 1µm is 100 percent, the results of them is not shown. The deposition efficiency of droplets with diameter of 0.3, 0.7 and 1 for inertial impactor with variable area simple, with oblique barrier located at 5 mm distance, with vertical barrier located at 5, 3 and 1 mm distance and with concave flexible plate and vertical barrier located at 1mm distance were increased respectively.

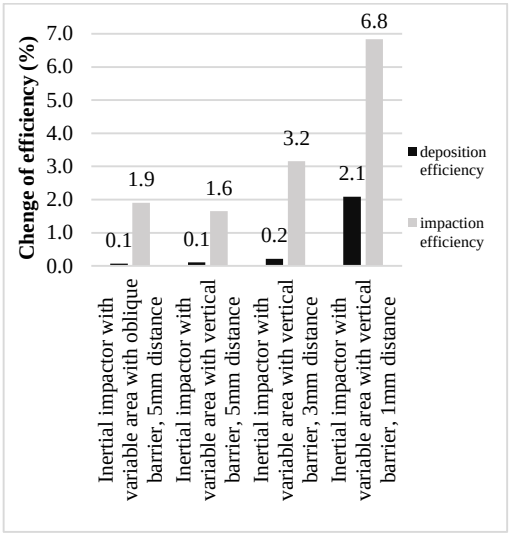

Fig. 24. Effect of using barriers at different distance in changing impaction and deposition efficiency numerically.

Fig. 24 shows the effect of using barrier in different distance versus the impaction and deposition efficiency in 8 L/min volumetric flow rate, numerically. In comparison with inertial impactor with variable area simple, using vertical barrier located at 5, 3 and 1 mm distance from outlet nozzle can give rise to an increase of 1.9, 3.16 and 6.83 percent in the impaction efficiency and an increase of 0.07, 0.22 and 2.09 percent in the deposition efficiency respectively. Also, using oblique barrier causes an increase of 0.65 percent in the impaction efficiency and an increase of 0.11 percent in the deposition efficiency. Because the speed of droplet is high, more than 60 percent of them after impact are rebounded.

3.1 Pressure Drops

Fig. 25 shows the pressure drops caused by using inertial impactor with variable area versus volumetric flow rate experimentally and numerically. In spite of the fact that the pressure drop caused by using oil separator in crankcase ventilation system must be less than 4 kpa, all kinds of designed inertial impactors with variable area pass this standard for volumetric flow rate less than 12 L/min. Using vertical and oblique barrier and concave flexible plate don't have a tangible effect on the pressure drop. The results show that the numerical simulations have good adaptation with the experimental results.

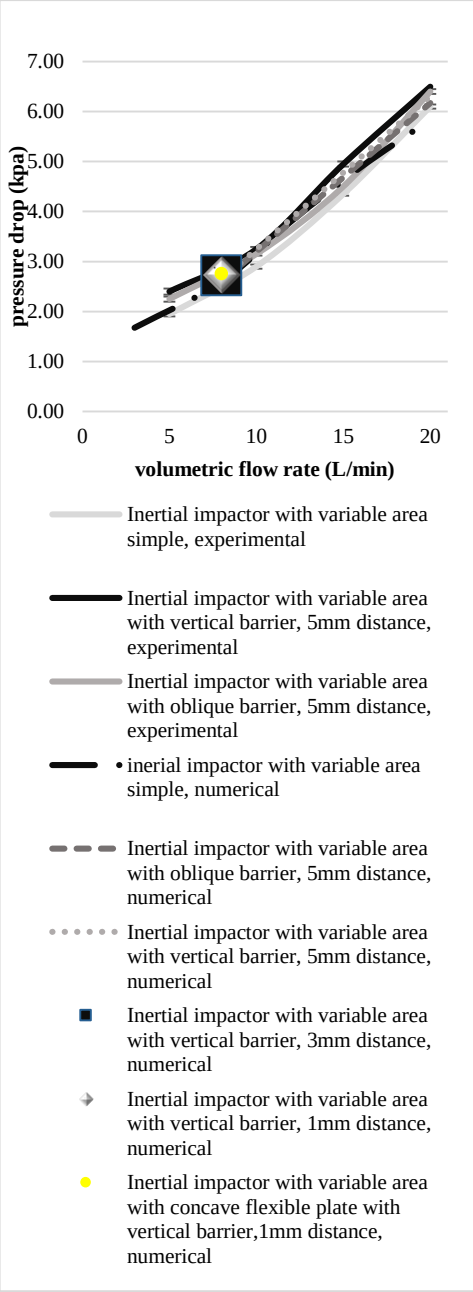

Fig. 25. Experimental and numerical pressure drops for inertial impactor with variable area.

4. CONCLUSION

In this paper, impaction and deposition efficiency of a micron-sized engine oil droplets on the inertial impactor with variable area is experimentally and numerically (3-D) studied as two different separate variables. The deposition and impaction efficiency for inertial impactor with variable area simple, with vertical barrier and oblique barrier are obtained more than 78 present for 8,12,16,20 L/min volumetric flow rate numerically and experimentally. The impaction and deposition efficiency are increased with increasing the volumetric flow rate. Although, vertical barrier is more effective than oblique barrier, using the barriers don't have noticeable effect on the deposition and impaction efficiency. According to the result, numerical simulation has good enough agreement with experimental data. The deposition efficiency for droplet with diameter more than 2 µm is obtained 100% numerically, these droplets are separated by flexible plate completely. Also about 90% of 1 µm droplets are separated by flexible plate and wall of exit channel. Most of the particles with diameter of 0.3 and 0.7 µm follow the carrier flow line. Exit channel plays a prominent role to separate the particles with diameter less than 1µm. The numerical results show that the deposition efficiency for particles with diameter less than 0.7 µm is less than 60 percent. The effect of distance between barrier and outlet of nozzle on impaction and deposition efficiency was considered numerically. As a result, using barriers across the flow can augment the impaction efficiency to 6 %. The result shows that with decreasing the distance between vertical barriers and outlet of nozzle, the efficiencies will be increased. The Pressure drop of the mentioned inertial impactor was on the range of admissible pressure of crankcase ventilation system for volumetric flow rate less than 12 L/min. using vertical and oblique barrier and concave flexible plate don't have noticeable effect on pressure drop.

ACKNOWLEDGMENTS

This study was sponsored by Iran Khodro Powertrain Company (IPCO). Authors would like to thank the Iran Khodro Powertrain Company (IPCO) for permission to use all of their equipment and laboratories.

5. APPENDIX

5.1 Computing of Displacement of the Lowest Part of Flexible Plate, Angle of Flexible Plate and the Hinge Location of Inertial Impactor with Variable Area

For numerical simulation it is necessary to know the angle of flexible plate in different volumetric flow rate. Fig. 26 shows three important parameter for numerical simulation in different volumetric flow rate that must be obtained by experimental tests.

- Displacement of the lowest part of flexible plate.
- Computing the angle of flexible plate.
- Computing the hinge location of the flexible plate.

- **Displacement of the Lowest Part of Flexible Plate**

A distance meter sensor (Wengler Sensor) was used to compute the displacement of the lowest part of flexible plate in different volumetric flow rate. At the first, the sensor must be calibrated. The calibration process is done by a stencil which

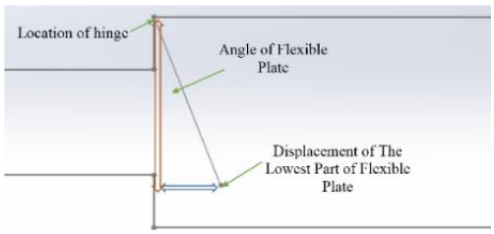

Fig. 26. Schematic of inertial impactor with variable area for computing the displacement of the lowest part of flexible plate, plate angle and hinge location.

contains some sheets with similar thickness. The location of sensor is fixed with an experimental peg which is shown in Fig. 27. The sensor is connected to the data acquisition device by a LAN cable and connected to a 24-volt power supply with another cable which is shown in Fig. 28. The power supply was used to provide the power of the sensor. The reported data from sensor was read by data acquisition device and then converted to the voltage by pulse data recorder software. After calibration, the distance meter sensor shows the 21.887mv equivalent of 1mm displacement. Then the experimental tests were started to compute the displacement of the lowest part of flexible plate which is shown in Fig.29. The fluid flow enters the inertial impactor with variable area after passing from the flow meter. By passing the flow through to the impactor plate, the flexible plate was opened and taken some distance from the nozzle's outlet. The distance is read by the distance meter sensor which is set on the bottom of the edge of plate.

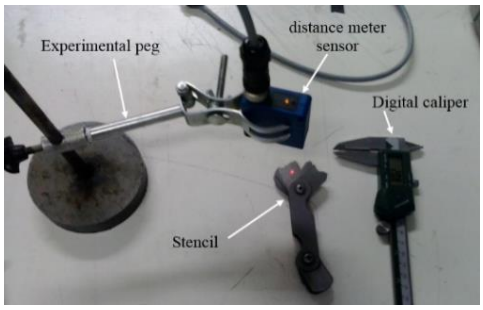

Fig. 27. Calibration of distance meter sensor.

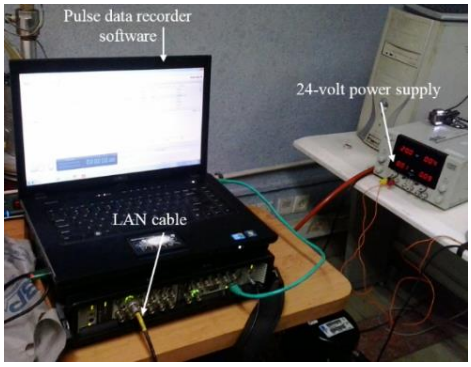

Fig. 28. Power supply, LAN cable, pulse data recorder software.

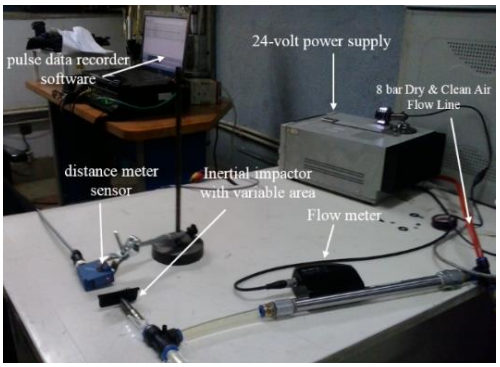

Fig. 29. Experimental setup to displacement of the lowest part of flexible plate.

Fig. 30 shows the displacement of the lowest part of flexible plate versus different volumetric flow rate experimentally. With using experimental data fitting, an equation is obtained to compute the plate displacement (Eq. 16).

$$y = 0.0356x - 0.0069 \quad (16)$$

Where y is the displacement of the lowest part of flexible plate (mm) and x is the inlet volumetric flow rate (L/min).

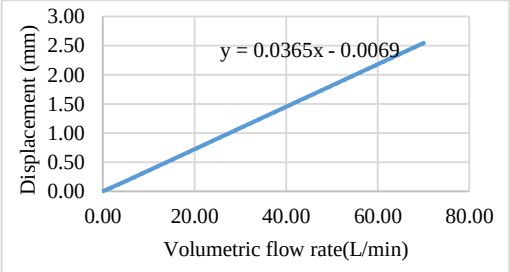

Fig. 30. Displacement of the lowest part of flexible plate versus different volumetric flow rate.

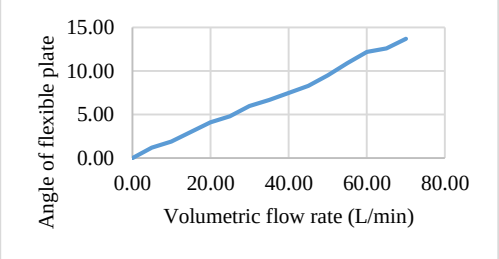

Fig. 31. Angle of flexible plate.

5.2 Computing the Angle of Flexible Plat

To compute the angle of flexible plate, the exit channel of inertial impactor must be cut out symmetrically. A camera was used to take a photo from beside the section in different volumetric flow rates (Fig. 32). The angle of flexible plate was computed by photo-shop software. As shown in Fig.32, the plate deflection was assumed linearly in order to use in numerical simulation.

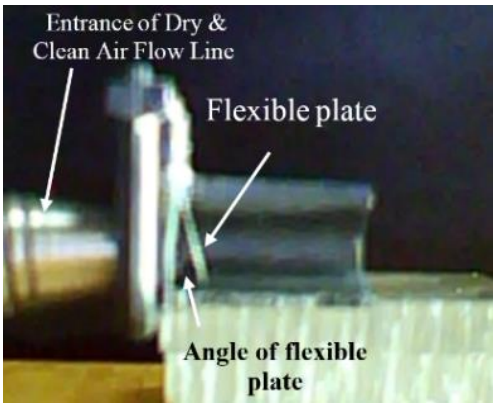

Fig. 32. Angle of flexible plate in 70 L/min volumetric flow rate.

5.3 Computing the hinge location of the flexible plate

Now, by obtaining the angle of flexible plate and displacement of lowest part of flexible plate, the hinge location of the flexible plate in every flow rate is computed by trigonometric relation (Eq. 17).

Hinge location =displacement of lowest part of flexible plate/ tanθ (17)

The hinge location of flexible plate is achieved 10.41mm by averaging all of the volumetric flow rate (Fig. 33).

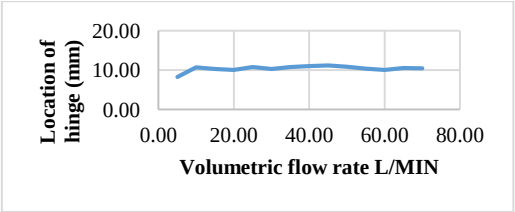

Fig. 33. Approximate hinge location of flexible plate toward volumetric flow rate.

Now by obtaining the above parameter, the numerical simulation is achievable.

REFERENCE

Alatawi, E. S., & Matida, E. A. (2012). Effect of anisotropy on particle deposition in impinging jet flow. *International Journal of Mechanical Engineering and Mechatronics*, 1(2), 95-101.

Arpandi, I., A. R. Joshi, O. Shoham, S. Shirazi and G. E. Kouba (1996). Hydrodynamics of two-phase flow in gas-liquid cylindrical cyclone separators. *SPE Journal* 1(04), 427-436.

Ashkenas, H. (1966). The structure and utilization of supersonic free jets in low density wind tunnels. *Proc. 4th International Symposium on Rarefied Gas Dynamics*.

Bazdidi-Tehrani, F., M. Karami and M. Jahromi (2011). Unsteady flow and heat transfer analysis of an impinging synthetic jet. *Heat and Mass Transfer* 47(11), 1363-1373.

Chen, H.-Y. and H.-L. Huang (2016). Numerical and experimental study of virtual impactor design and aerosol separation. *Journal of Aerosol Science* 94, 43-55.

Crowe, C. T., J. D. Schwarzkopf, M. Sommerfeld and Y. Tsuji (2011). *Multiphase flows with droplets and particles*, CRC press.

de la Mora, J. F., S. Hering, N. Rao and P. McMurry (1990). Hypersonic impaction of ultrafine particles. *Journal of Aerosol Science* 21(2), 169-187.

De La Mora, J. F., N. Rao and P. McMurry (1990). Inertial impaction of fine particles at moderate Reynolds numbers and in the transonic regime with a thin-plate orifice nozzle. *Journal of Aerosol Science* 21(7), 889-909.

Ehteram, M. A., H. B. Tabrizi, G. Ahmadi, M. Safari and M. A. Mirsalim (2013). Investigation of fine droplet generation from hot engine oil by impinging gas jets onto liquid surface. *Journal of Aerosol Science* 65, 49-57.

Ehteram, M. A., H. B. Tabrizi, M. Mesbah, G. Ahmadi and M. A. Mirsalim (2012). Experimental study on the effect of connecting ducts on demisting cyclone efficiency. *Experimental Thermal and Fluid Science* 39, 26-36.

Feng, J., Y. Chang, X. Peng and Z. Qu (2008). Investigation of the oil—gas separation in a horizontal separator for oil-injected compressor units. *Proceedings of the Institution of Mechanical Engineers, Part A: Journal of Power and Energy* 222(4), 403-412.

Forney, L. (1991). Particle impaction in axially symmetric supersonic flow. *Aerosol Science and Technology* 15(1), 49-59.

Hering, S. V., R. C. Flagan and S. K. Friedlander (1978). Design and evaluation of new low-pressure impactor. I. *Environmental Science and Technology* 12(6), 667-673.

Hutchinson, P., G. Hewitt and A. Dukler (1971). Deposition of liquid or solid dispersions from turbulent gas streams: a stochastic model. *Chemical Engineering Science* 26(3), 419-439.

Ishii, R., Y. Umeda and M. Yuhi (1989). Numerical analysis of gas-particle two-phase flows. *Journal of fluid mechanics* 203, 475-515.

Issa, R. I. (1986). Solution of the implicitly discretised fluid flow equations by operator-splitting. *Journal of computational physics* 62(1), 40-65.

Kallio, G. and M. Reeks (1989). A numerical simulation of particle deposition in turbulent boundary layers. *International Journal of Multiphase Flow* 15(3), 433-446.

Kim, M. K., W. G. Kim, K.-S. Lee and S.-J. Yook (2014). Collection efficiency of round-nozzle

impactors with horizontal annular inlet. *Journal of Aerosol Science* 74, 63-69.

Menter, F. R. (1994). Two-equation eddy-viscosity turbulence models for engineering applications. *AIAA Journal* 32(8), 1598-1605.

Movafaghian, S., J. Jaua-Marturet, R. S. Mohan, O. Shoham and G. Kouba (2000). The effects of geometry, fluid properties and pressure on the hydrodynamics of gas–liquid cylindrical cyclone separators. *International Journal of Multiphase Flow* 26(6), 999-1018.

Oh, J. J. and S. S. Kim (1994). Particle deposition on a truncated cylinder in a supersonic flow at low pressure. *Aerosol Science and Technology* 20(4), 375-384.

Pagnozzi, R. M., D. C. Pereira, L. Spielmann and P. Bastías (2007). Methodology applied on the validation of air/oil separation systems integrated to the crankcase ventilation valve, *SAE Technical Paper*.

Petkov, J. T., N. D. Denkov, K. D. Danov, O. D. Velev, R. Aust and F. Durst (1995). Measurement of the drag coefficient of spherical particles attached to fluid interfaces. *Journal of colloid and interface science* 172(1), 147-154.

Rajmistry, S., S. Ganguli, P. Chandra and P. K. Chatterjee (2017). Numerical Analysis of Gas-Solid Behavior in a Cyclone Separator for Circulating Fluidized Bed System. *Journal of Applied Fluid Mechanics* 10(4).

Saffman, P. (1965). The lift on a small sphere in a slow shear flow. *Journal of Fluid Mechanics* 22(2), 385-400.

Satoh, K., T. Kawai, M. Ishikawa and T. Matsuoka (2000). Development of method for predicting efficiency of oil mist separators, *SAE Technical Paper*.

Shojaeefard, M. H., V. M. Khaneshan, M. A. Ehteram, M. Akbari and E. Allymehr (2015). Taguchi optimization of micron sized lubricant oil droplet deposition on a hot plate. *Journal of Mechanical Science and Technology* 29(8): 3277-3285.

Shojaeefard, M. H., V. M. Khaneshan, M. R. Yosri, M. A. Ehteram and E. Allymehr (2016). Investigation of engine oil micro-droplets deposition using a round impinging jet. *Journal of the Brazilian Society of Mechanical Sciences and Engineering* 38(3), 721-734.

Shukla, S. K., P. Shukla and P. Ghosh (2011). Evaluation of numerical schemes for dispersed phase modeling of cyclone separators. *Engineering Applications of Computational Fluid Mechanics* 5(2), 235-246.

Wilcox, D. C. (2008). Formulation of the kw turbulence model revisited. *AIAA journal* 46(11), 2823-2838.